

Polymorphism and Phase Transitions in Layered Uranium(VI) Hydroxides: Ab Initio Lattice Dynamics Simulations of $\text{UO}_2(\text{OH})_2$

Philippe F. Weck^{†a} and Eunja Kim^b

^a Sandia National Laboratories, Albuquerque, NM 87185, USA. † E-mail: pfweck@sandia.gov.

^b Department of Physics, The University of Texas at El Paso, 500 W University, El Paso, Texas 79902, USA.

The phase transitions and thermodynamics of stoichiometric α -, β -, and γ - $\text{UO}_2(\text{OH})_2$ polymorphs are investigated using density functional perturbation theory (DFPT). The pressure-induced $\beta(Pbca) \rightarrow \alpha(Cmca)$ phase transition is reproduced by calculations, with a volume reduction of $\Delta V/V = -14.7\%$ similar to experiment. Consistent with observation, a temperature-driven $\gamma(P2_1/c) \rightarrow \beta(Pbca)$ phase transition is predicted near 533 K. At 298.15 K, the computed standard molar heat capacity of α - $\text{UO}_2(\text{OH})_2$ is $C_p^0 = 112.1 \text{ J}\cdot\text{mol}^{-1}\cdot\text{K}^{-1}$, only 1.6% smaller than the value of $C_p^0 = 113.96 \pm 0.12 \text{ J}\cdot\text{mol}^{-1}\cdot\text{K}^{-1}$ measured by calorimetry. $C_p^0 = 112.4$ and $104.8 \text{ J}\cdot\text{mol}^{-1}\cdot\text{K}^{-1}$ are predicted for the β - and γ - $\text{UO}_2(\text{OH})_2$ polymorphs, respectively. The calculated molar enthalpy and Gibbs energy functions of the α -, β - and γ - $\text{UO}_2(\text{OH})_2$ polymorphs are also reported.

Introduction

Understanding the relative stability and structure-property relationships of uranyl-bearing materials is of paramount importance to determine the paragenesis and chemical evolution of uranium minerals in the environment. In particular, predicting the fate of uranyl alteration phases produced from spent nuclear fuel (SNF) degradation is crucial to assess the overall performance and safety of deep geological repositories for the disposal of long-lived radioactive waste.^{1,2,3,4} While uranium transport in the environment is limited under reducing conditions, oxidative dissolution of UO_2 by weathering can occur relatively fast and release significant amounts of uranyl ions (UO_2^{2+}) in geochemical fluids. This process can greatly accelerate the mobility of U(VI) molecular complexes in highly oxidizing aqueous environments.

Change in solution chemistry from oxidizing to reducing conditions leads to the precipitation of various uranyl phases, with chemical composition and structures depending on the local environment. Uranyl oxide hydrates and hydroxides represent an important subgroup of mineral phases formed upon precipitation of hexavalent uranium. These minerals typically crystallize as polyhedral sheets with composition $[(\text{UO}_2)_x\text{O}_y(\text{OH})_z]^{(2x-2y-z)}$.^{5,6,7,8} Among uranyl oxide hydrate and hydroxide minerals without cations in their interlayer space, schoepite, metaschoepite and dehydrated schoepite are topologically related. The structures of schoepite, $[(\text{UO}_2)_8\text{O}_2(\text{OH})_{12}] \cdot 12\text{H}_2\text{O}$ (or $\text{UO}_3 \cdot 2.25\text{H}_2\text{O}$), and metaschoepite

$(\text{UO}_2)_8\text{O}_2(\text{OH})_{12}] \cdot 10\text{H}_2\text{O}$ (or $\text{UO}_3 \cdot 2\text{H}_2\text{O}$), consist of edge-sharing UO_7 pentagonal bipyramids, arranged as $(\text{UO}_2)_4\text{O}(\text{OH})_6$ sheets, and only slightly differ by their uranyl group orientation relative to the layers.^{9,10} Dehydrated schoepite was suggested to form an omission solid-solution with a general formula $(\text{UO}_2)\text{O}_{0.25-x}(\text{OH})_{1.5+2x}$ ($0 \leq x \leq 0.25$) (or $\text{UO}_3 \cdot x\text{H}_2\text{O}$ ($0.75 \leq x \leq 1$)). The stoichiometric dehydrated schoepite phase, α - $\text{UO}_2(\text{OH})_2$, is made of edge-sharing UO_8 hexagonal bipyramids arranged as $\text{UO}_2(\text{OH})_2$ sheets.^{11,12} Both schoepite and metaschoepite structures were shown to be related to α - $\text{UO}_2(\text{OH})_2$ by the substitution $2(\text{OH}) = \text{O}^{2-} + \text{vacancy}$ in uranyl sheets.¹²

The alteration of schoepite – the most thermodynamically stable corrosion product formed upon UO_2 dissolution – to dehydrated schoepite occurs through a multistep process. Following the initial loss of interlayer H_2O , atomic rearrangement occurs within sheets to produce a metaschoepite-like structure, with a final rearrangement to a α - $\text{UO}_2(\text{OH})_2$ -type sheet structure.¹² Dehydration of schoepite to α - $\text{UO}_2(\text{OH})_2$ can occur rapidly in air at ambient temperature or slowly in water or humidity around $\sim 100^\circ\text{C}$.¹² The 3% unit-cell volume decrease and H-bonds rearrangement accompanying the slow transformation of schoepite ($V_0 = 3551.2 \text{ \AA}^3$, space group $P2_1ca$) into metaschoepite ($V_0 = 3445.5 \text{ \AA}^3$, space group $Pbna$) do not produce enough strain energy to fully convert $\text{UO}_3 \cdot 2.25\text{H}_2\text{O}$ to $\text{UO}_3 \cdot 2\text{H}_2\text{O}$. However, this excess strain energy is sufficient to initiate to the fast transformation of residual schoepite into dehydrated schoepite, when altered crystals are exposed to moderate external stress.¹² Upon contact with moisture and H_2O_2 produced by water α -radiolysis near the UO_2 surface,^{13,14,15} dehydrated schoepite can rapidly transform into the mineral studtite, $(\text{UO}_2)_2\text{O}_2(\text{H}_2\text{O})_4$, another corrosion phase resulting from SNF degradation.^{12,16,17,18,19}

^a Sandia National Laboratories, Albuquerque, NM 87185, USA.

^b Department of Physics, The University of Texas at El Paso, 500 W University, El Paso, Texas 79902, USA.

† E-mail: pfweck@sandia.gov.

While the structural relationships and stability fields of schoepite, metaschoepite and dehydrated schoepite have been extensively investigated, only limited information is available on $\text{UO}_2(\text{OH})_2$ polymorphs. Early experimental investigations showed that $\text{UO}_2(\text{OH})_2$ can be synthesized hydrothermally from UO_3 and H_2O , resulting in the distinct crystalline α , β and γ polymorphs.^{20,21} Using X-ray diffraction (XRD) and neutron scattering methods, the crystal parameters of these polymorphs were determined in the seminal studies by Taylor et al.^{11,22,23,24} and others.^{25,26} Based on experimental studies and natural occurrences,^{5,27} Finch et al. predicted the approximate thermal stability fields of α -, β - and γ - $\text{UO}_2(\text{OH})_2$ polymorphs in water (with H_2O activity of $a_w=1$), i.e., ~ 95 – 125°C for γ , ~ 95 – 325°C for β , and ~ 95 – 345°C for α .¹² All three polymorphs might exist under potential thermal conditions of interest for SNF and uranium-containing nuclear waste disposal in geological repositories. The mineral Paulscherrite, with a simplified structural formula $\text{UO}_2(\text{OH})_2$, was recently identified as dehydrated schoepite crystallizing in the monoclinic symmetry (pseudo-orthorhombic, with $P2_1$, $P2_1/m$, or $P2_1/m$ space group). Paulscherrite is isostructural with synthetic α - $\text{UO}_2(\text{OH})_2$, adopting the orthorhombic $Cmca$ space group symmetry.^{11,23,28}

Two phase transitions were reported in early experimental studies of $\text{UO}_2(\text{OH})_2$ polymorphs, namely a temperature-driven $\gamma \rightarrow \beta$ irreversible phase transition in the vicinity of 125°C ,²⁶ and a pressure-induced $\beta \rightarrow \alpha$ martensitic-like phase transformation with a volume of contraction of *ca.* 14%.^{24,29,30} To the best of our knowledge, phase transitions between $\text{UO}_2(\text{OH})_2$ polymorphs have never been investigated using computational methods. In addition, the thermodynamic properties of $\text{UO}_2(\text{OH})_2$ were studied experimentally with a focus on the α and β polymorphs.^{31,32,33,34} However, discrepancies of up to $\sim 18\%$ were found between the standard molar entropy values derived from differential scanning calorimetry (DSC) measurements by Hemingway³² and the calorimetry measurements by O'Hare *et al.*³³ or the value estimated from Latimer's rule by Cordfunke and O'Hare.³¹ The thermodynamic functions of stoichiometric $\text{UO}_2(\text{OH})_2$ were also computed by Weck and Kim³⁵ and Colmenero *et al.*³⁶ using first-principles methods, but were limited to the α phase.

In this work, the crystal structures and thermodynamic properties of the α -, β - and γ - $\text{UO}_2(\text{OH})_2$ polymorphs, as well as the pressure-induced $\beta \rightarrow \alpha$ phase transition and temperature-driven $\gamma \rightarrow \beta$ phase transition, are investigated within the framework of density functional theory (DFT). Details of the computational methods utilized in this study are given in the next section, followed by a discussion of our results and conclusions.

Computational methods

Total energy calculations were conducted using spin-polarized DFT implemented in the Vienna Ab initio Simulation Package (VASP).³⁷ The exchange-correlation energy was computed within the generalized gradient approximation³⁸ (GGA), with the parameterization of Perdew, Burke, and Ernzerhof³⁹ (PBE).

Previous studies showed that standard density functionals, such as the PBE or PW91 functionals, correctly describe the structural parameters and properties of uranium oxides and uranium compounds characterized experimentally.^{35,36,40,41,42,43,44,45,46,47} While computational approaches beyond standard DFT are often required to account for strong on-site Coulomb repulsion between uranium 5f electrons (e.g. in $^{IV}\text{UO}_2$), previous DFT investigations of crystalline uranyl oxide hydrates and hydroxides (e.g., schoepite, metaschoepite and dehydrated schoepite) demonstrated that standard DFT is sufficient describe these systems.^{35,36,45,48,49}

The projector augmented wave (PAW) method was used to describe the interaction between valence electrons and ionic cores.^{50,51} In the Kohn-Sham (KS) equations, U(6s,6p,6d,5f,7s) and O(2s,2p) electrons were treated explicitly as valence electrons and the remaining core electrons, together with the nuclei, were represented by PAW pseudopotentials. Davidson's⁵² blocked iterative matrix diagonalization scheme was used to solve the KS equations. The plane-wave energy cutoff for the electronic wavefunctions was set to 500 eV, ensuring convergence of the total energy of the system to within 1 meV/atom.

The crystal structures of α -, β - and γ - $\text{UO}_2(\text{OH})_2$ polymorphs were optimized with 3D-periodic boundary conditions applied. Ionic relaxation was carried out using the quasi-Newton method and the Hellmann-Feynman forces acting on atoms were calculated with a convergence tolerance set to 0.01 eV/Å. Structure optimization and properties calculations were carried out using the Monkhorst-Pack special k -point scheme⁵³ with $5 \times 3 \times 5$, $5 \times 5 \times 3$ and $5 \times 5 \times 5$ meshes for integrations in the Brillouin zone (BZ) of the bulk α -, β -, and γ - $\text{UO}_2(\text{OH})_2$ polymorphs, respectively. The tetrahedron method with Blöchl corrections⁵⁴ was used for BZ integrations. Periodic unit cells containing 28 atoms ($Z = 4$) for the α and β phases and 14 atoms ($Z = 2$) for the γ phase were used in the calculations. Based on previous studies of uranyl crystal structures with various cell sizes, the size of the 3D-periodic simulation cells does not significantly impact the accuracy of the calculations.^{35,36,43,44,45,47,48,49} Ionic and cell relaxations of the experimental bulk structures^{11,22,24,26}, used as initial guesses, were performed simultaneously, without symmetry constraints applied.

Density functional perturbation theory (DFPT) implemented in VASP was used to compute the forces exerted on atoms of the bulk α -, β -, and γ - $\text{UO}_2(\text{OH})_2$ structures and phonon frequencies were derived. Phonon analysis was performed at constant equilibrium volume to derive the Helmholtz free energy, calculated according to:

$$F(T) = \frac{1}{2} \sum \hbar \omega + k_B T \sum \ln[1 - e^{-\beta \hbar \omega}], \quad (1)$$

where \hbar is the reduced Planck constant, $\hbar \omega$ is the energy of a single phonon with angular frequency ω , k_B is the Boltzmann constant, T is the temperature of the system, and $\beta = (k_B T)^{-1}$. Thermal properties at constant pressure (e.g., the Gibbs free energy and the isobaric heat capacity) were predicted within the quasi-harmonic approximation (QHA), based on a set of phonon calculations in the vicinity of the computed equilibrium

crystal structures. The QHA introduces a volume dependence of phonon frequencies as a part of anharmonic effect.⁵⁵ All the thermodynamic properties were obtained using the Phonopy software.⁵⁵ Within the QHA, the Gibbs free energy is defined at a constant pressure by the transformation:

$$G(T, p) = \min_V [U(V) + F(T; V) + pV], \quad (2)$$

where \min_V [function of V] corresponds to a unique minimum of the expression between brackets with respect to the volume V , U is the total energy of the system, and p is the pressure applied. The isobaric molar heat capacity versus temperature was calculated as the second derivative of the Gibbs free energy with respect to the temperature T :

$$C_p(T) = -T \frac{\partial^2 G}{\partial T^2}. \quad (3)$$

The molar entropy was obtained by integration of the isobaric molar heat capacity:

$$S(T) = \int \frac{C_p(T)}{T} dT. \quad (4)$$

Results and discussion

Crystal structures

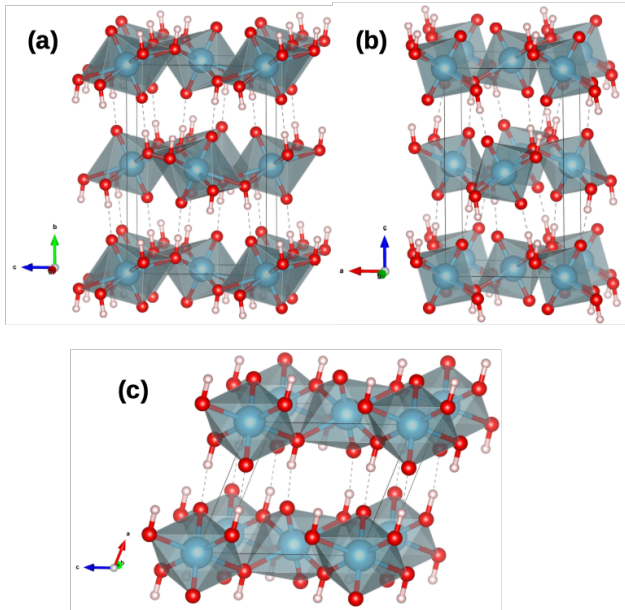


Fig. 1 Crystal unit cells of (a) α - $\text{UO}_2(\text{OH})_2$ ($Z = 4$, space group $Cmca$), (b) β - $\text{UO}_2(\text{OH})_2$ ($Z = 4$, space group $Pbca$), (c) γ - $\text{UO}_2(\text{OH})_2$ ($Z = 2$, space group $P2_1/c$), relaxed with DFT at the GGA/PBE level of theory. O-H...O(uranyl) hydrogen bonds are represented by dashed lines and U coordination polyhedra are also displayed. Color legend: U, blue; O, red; H, white.

The equilibrium crystal unit cells of α -, β - and γ - $\text{UO}_2(\text{OH})_2$ polymorphs relaxed with DFT at the GGA/PBE level of theory are shown in Fig. 1. The optimized lattice parameters are $a = 4.233$ Å, $b = 10.344$ Å, $c = 6.970$ Å, $\alpha = \beta = \gamma = 90^\circ$, $V = 305.2$ Å³ ($Z = 4$,

space group $Cmca$, IT No. 64) for orthorhombic α - $\text{UO}_2(\text{OH})_2$, $a = 5.848$ Å, $b = 6.204$ Å, $c = 9.867$ Å, $\alpha = \beta = \gamma = 90^\circ$, $V = 358.0$ Å³ ($Z = 4$, space group $Pbca$, IT No. 61) for orthorhombic β - $\text{UO}_2(\text{OH})_2$, and $a = 5.891$ Å, $b = 5.322$ Å, $c = 6.369$ Å, $\alpha = \gamma = 90^\circ$, $\beta = 113.8^\circ$, $V = 182.73$ Å³ ($Z = 2$, space group $P2_1/c$, IT No. 14) for monoclinic γ - $\text{UO}_2(\text{OH})_2$. These optimized structures are in overall good agreement with the polymorph structures characterized originally from XRD and neutron scattering techniques by Taylor and co-workers^{11,22,23,24} and others^{25,26} (see Table 1).

Table 1. Structural parameters of α -, β - and γ - $\text{UO}_2(\text{OH})_2$ polymorphs.

α phase	a (Å)	b (Å)	c (Å)	β (°)	V (Å ³)	Symmetry
DFT ^{a,b}	4.233	10.344	6.970	90	305.2	$Cmca$
DFT-D2 ^b	4.222	10.304	6.938	90	301.8	$Cmca$
DFT-D2 ^c	4.2309	10.3104	6.9195	90	301.87	$Cmca$
Expt. ^d	4.242(1)	10.302(1)	6.868(1)	90	300.1(1)	$Cmca, C2cb$
Expt. ^e	4.2455(6)	10.3183(16)	6.8648(10)	90	300.7(1)	$Cmca, C2cb$
Expt. ^f	4.288(2)	10.270(6)	6.885(5)	90.39	303.2(2)	$P2_1, P2_1, P2_1/m$
β phase	a (Å)	b (Å)	c (Å)	β (°)	V (Å ³)	Symmetry
DFT ^a	5.848	6.204	9.867	90	358.0	$Pbca$
Expt. ^g	5.6438(1)	6.2867(1)	9.9372(2)	90	352.6(1)	$Pbca$
Expt. ^h	5.635(7)	6.285(8)	9.919(8)	90	351.3	$Pbca$
γ phase	a (Å)	b (Å)	c (Å)	β (°)	V (Å ³)	Symmetry
DFT ^a	5.891	5.322	6.369	113.8	182.7	$P2_1/c$
Expt. ⁱ	5.560(3)	5.522(3)	6.416(3)	112.71	181.7(5)	$P2_1/c$

^aThis study; ^bWeck and Kim, 2014; ^cColmenero *et al.*, 2018; ^dTaylor, 1971;

^eTaylor, Kelly and Downer, 1972; ^fBrugger *et al.*, 2011, mineral

Paulscherrite approximately isostructural with α - $\text{UO}_2(\text{OH})_2$; ^gBannister and Taylor, 1970; ^hRoof *et al.*, 1964; ⁱSiegel *et al.*, 1972.

In the α phase, the $\text{UO}_2(\text{OH})_2$ layers are linked by O-H...O (uranyl) hydrogen bonds and the uranium coordination number is eight, with a puckered hexagonal arrangement.²³ In the β phase, the uranium centers possess a coordination of six in with octahedral arrangement and the stacked $\text{UO}_2(\text{OH})_2$ layers are also linked by O-H...O (uranyl) hydrogen bonds.²² The location of hydrogen atoms in the α and β phases were confirmed by the neutron powder diffraction studies of Taylor and Hurst.¹¹ In the γ phase, the configuration about uranium atoms is a distorted coordination octahedron with variable U-O distances and the overall structure shows strong similarity to β - $\text{UO}_2(\text{OH})_2$.

The b/a and c/a ratios calculated with DFT are, respectively, 2.444 and 1.646 for the α phase, 1.061 and 1.687 for the β phase, and 0.903 and 1.081 for the γ phase. These ratios are close to the corresponding experimental values of 2.429 and 1.619 for the α phase characterized by Taylor²³ ($a = 4.242(1)$ Å, $b = 10.302(1)$ Å, $c = 6.868(1)$ Å, $V = 300.1(1)$ Å³), 1.114 and 1.761 for the β phase reported by Bannister and Taylor²² ($a = 5.6438(1)$ Å, $b = 6.2867(1)$ Å, $c = 9.9372(2)$ Å, $V = 352.6(1)$ Å³), and 0.957 and 1.154 for the γ phase solved by Siegel *et al.*²⁶ ($a = 5.560(3)$ Å, $b = 5.522(3)$ Å, $c = 6.416(3)$ Å, $V = 181.7(5)$ Å³). The equilibrium unit-cell volumes of α -, β - and γ - $\text{UO}_2(\text{OH})_2$ predicted with DFT are ca. 1.7%, 1.5%, and 1.1% larger, respectively, than experimental estimates, owing to the tendency of GGA-type functionals to overestimate bond distances.

In addition, since dehydrated schoepite polymorphs are made of stacked $\text{UO}_2(\text{OH})_2$ layers linked by $\text{O}-\text{H}\cdots\text{O}(\text{uranyl})$ hydrogen bonds (Fig. 1), previous first-principles studies of the α phase utilized DFT corrected for dispersion⁵⁶ (DFT-D) to account more accurately for long-range interactions between adjacent sheets.^{35,36} The DFT-D method of Grimme⁵⁷ (DFT-D2) used in those studies slightly improves the agreement between calculated and experimental lattice parameters at low temperature (see Table 1). This method describes dispersion interactions resulting from dynamical correlations between fluctuating charge distributions *via* a simple semi-empirical pair-wise force field potential. The DFT-D2 calculation of the α - $\text{UO}_2(\text{OH})_2$ interlayer spacing (*i.e.*, $b/2 = 5.152 \text{ \AA}$) essentially reproduces the value of $b/2 = 5.151 \text{ \AA}$ measured by Taylor¹¹ and reduces the difference between measured and computed unit cell volumes to $\sim 0.6\%$. However, simple semi-empirical pair-wise force field potentials used to represent dispersion interactions in DFT-D2 are typically optimized for low-temperature crystalline structures. This may lead to inaccurate prediction of thermal properties at higher temperature. For this reason, standard DFT was used in the remainder of this study.

Energetics of $\text{UO}_2(\text{OH})_2$ polymorphs

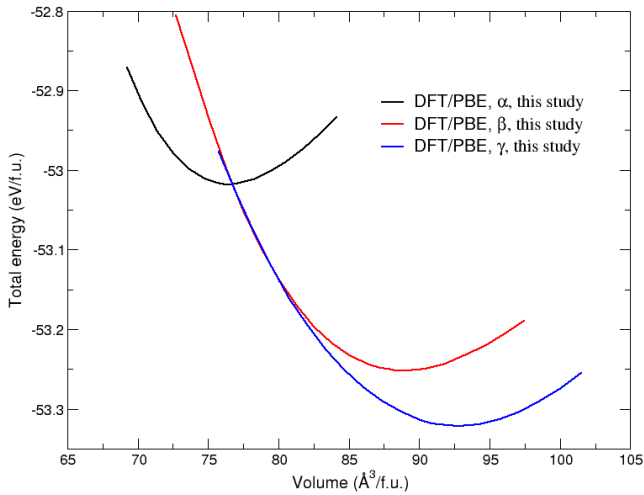


Fig. 2 Variation of the total energy as a function of the crystal volume per formula unit (f.u.) of α -, β - and γ - $\text{UO}_2(\text{OH})_2$ polymorphs calculated at 0 K with DFT at the GGA/PBE level of theory.

Fig. 2 shows the evolution of the total energy U as a function of the crystal volume per formula unit (f.u.) of α -, β - and γ - $\text{UO}_2(\text{OH})_2$ polymorphs predicted with DFT at the athermal limit. Calculations predict that monoclinic γ , with the largest equilibrium volume, is the most energetically stable phase, followed by the orthorhombic β phase, and the orthorhombic α phase. The pressure-induced $\beta \rightarrow \alpha$ and $\gamma \rightarrow \alpha$ phase transitions, from open octahedral structures with six O atoms coordinated to uranium metal centers to puckered hexagonal sheets with 8-coordinated uranium atoms, lead to theoretical volume reductions of $\Delta V/V = -14.7\%$ and -16.4% , respectively. This result exactly matches the volume contraction value for the $\beta \rightarrow \alpha$ martensitic-like phase transformation measured by Taylor *et al.*²⁴ using dilatometry and XRD techniques. The $\beta \rightarrow \alpha$ transformation occurs by shear deformation, without breaking hydrogen bonds, with a slip of $\sim 1 \text{ \AA}$ between the $\text{UO}_2(\text{OH})_2$ layers and

with the line of demarcation of the α and β phase lying in the diagonal plane, since the edges of both phases are of the type $\{111\}$.²⁴ This $\beta \rightarrow \alpha$ phase transition taking place along a $\langle 110 \rangle$ dipyrmaid direction appears to fit Buerger's displacive transformation classification.²⁹

Moreover, the present finding that γ and β polymorphs become energetically degenerate upon volume contraction, as they convert to the α polymorph, explains the grinding experiments of Siegel and co-workers²⁶ postulating the existence of a shear relationship between the γ and β structures. In these experiments, it was found that, on the one hand, grinding β -phase crystals resulted in pressure-induced conversion to α phase, together with a minor amount of γ phase. On the other hand, grinding γ -phase crystals also led to the formation of α phase, with small amount of β phase. Complete conversion to the high-density α phase was eventually achieved by continued grinding of either β - or γ - $\text{UO}_2(\text{OH})_2$ starting materials.

Thermodynamic properties

The thermal properties, *i.e.*, Gibbs free energy, isobaric heat capacity, entropy, enthalpy and Gibbs energy functions, of bulk α -, β -, and γ - $\text{UO}_2(\text{OH})_2$ were obtained from DFPT calculations, used to compute the forces exerted on atoms of the bulk polymorph structures and associated phonon frequencies.

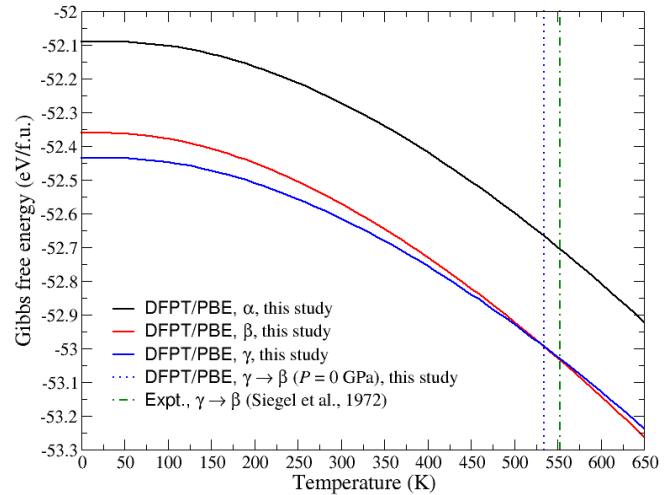


Fig. 3 Variation of the Gibbs free energy as a function of the crystal unit-cell volume per formula unit (f.u.) of α -, β - and γ - $\text{UO}_2(\text{OH})_2$ polymorphs calculated with DFPT at the GGA/PBE level of theory. The $\gamma \rightarrow \beta$ phase transition temperature observed by Siegel *et al.* (Ref. 26) (green dash-dotted line) is indicated for comparison with the present DFPT/PBE results (blue dotted line).

Fig. 3 displays the thermal variation of the Gibbs free energy (Eq. 2) of bulk α -, β -, and γ - $\text{UO}_2(\text{OH})_2$ predicted with DFPT. Similar to the evolution of the total energy in Fig. 2, γ - $\text{UO}_2(\text{OH})_2$ is the lowest-energy, most stable phase at low temperature, in line with the expectation that the least dense polymorph shows increased stability relative to denser polymorphs.²⁶ DFT calculations show a temperature-driven $\gamma \rightarrow \beta$ phase transition occurs in the vicinity of $\sim 533 \text{ K}$, in good agreement with the experimental observation by Siegel *et al.*,²⁶ who reported a major change of the crystal unit-cell angle from $\beta = 112.71^\circ$ in $P2_1/c$ γ - $\text{UO}_2(\text{OH})_2$ to a value close to 90° in $Pbca$ β - $\text{UO}_2(\text{OH})_2$

above ~ 553 K ($\sim 280^\circ\text{C}$). The relatively small differences in computed Gibbs free energy between γ and β phases in the temperature range ~ 400 – 650 K suggest that the $\gamma \rightarrow \beta$ transition is rather sluggish, consistent with thermo-analytical experiments indicating that the γ phase may start slowly converting to the β phase at temperatures as low as ~ 400 K ($\sim 125^\circ\text{C}$).²⁶

The thermal evolution of the isobaric molar heat capacity, C_p , calculated with DFPT for stoichiometric bulk α -, β -, and γ - $\text{UO}_2(\text{OH})_2$ polymorphs is depicted in Fig. 4. Excellent agreement is obtained between the isobaric molar heat capacity calculated in this study for α - $\text{UO}_2(\text{OH})_2$ and the corresponding calorimetry data of Gurevich *et al.*³⁴ in the temperature range 14–316 K. At 298.15 K, the predicted standard molar heat capacity is $C_p^0 = 112.1$ J.mol⁻¹.K⁻¹, i.e., underestimating the experimental value of $C_p^0 = 113.96 \pm 0.12$ J.mol⁻¹.K⁻¹ measured by Gurevich *et al.*³⁴ by only 1.6%. However, this computed C_p^0 value is 2.8% larger than the value of 109.0 J.mol⁻¹.K⁻¹ estimated by Hemingway for stoichiometric α - $\text{UO}_2(\text{OH})_2$ (i.e., $\text{UO}_3 \cdot \text{H}_2\text{O}$), extrapolated from DSC measurement of dehydrated schoepite as $\text{UO}_3 \cdot 0.77\text{H}_2\text{O}$.³² Indeed, Hemingway reported in the temperature range 298.15–700 K such experimental heat capacity estimates of α -type dehydrated schoepite corrected to the compositions of $\text{UO}_3 \cdot 0.85\text{H}_2\text{O}$ and $\text{UO}_3 \cdot \text{H}_2\text{O}$ through addition of the heat capacity of the appropriate amount of H_2O as steam at the temperature of the experimental data point.³² As pointed in calorimetry experiments, dehydrated schoepite can have various hydration levels, with observed compositions typically in the range $(\text{UO}_2)\text{O}_{0.25-x}(\text{OH})_{1.5+2x}$ ($0 \leq x \leq 0.25$) [or $\text{UO}_3 \cdot x\text{H}_2\text{O}$ ($0.75 \leq x \leq 1$)].^{12,32} For example, thermal gravimetric analysis (TGA) indicated that the composition of dehydrated schoepite is approximately $\text{UO}_3 \cdot 0.8\text{H}_2\text{O}$ in the temperature range 293–413 K,²⁰ while other differential gravimetric analyses (DGA) and TGA studies showed that dehydrated schoepite corresponds to $\text{UO}_3 \cdot 0.75\text{H}_2\text{O}$ up to ca. 450 K.^{29,58,59}

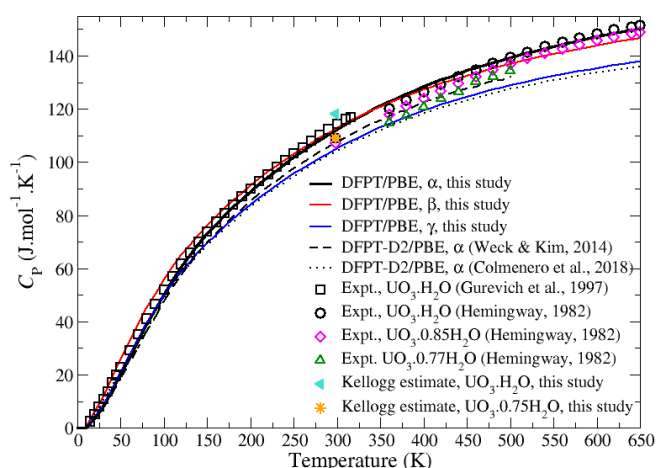


Fig. 4 Thermal variation of the isobaric molar heat capacity of α -, β - and γ - $\text{UO}_2(\text{OH})_2$ polymorphs calculated with DFPT at the GGA/PBE level of theory. DFPT-D/GGA/PBE calculations for α - $\text{UO}_2(\text{OH})_2$ (Weck and Kim, 2014) and calorimetry estimates for α -type $\text{UO}_3 \cdot x\text{H}_2\text{O}$ ($x = 0.77, 0.85, 1.00$) are also shown for comparison purpose (Hemingway, 1982; Gurevich *et al.*, 1997).

To estimate standard C_p^0 values over the full compositional range $\text{UO}_3 \cdot 0.75\text{H}_2\text{O}$ to $\text{UO}_3 \cdot \text{H}_2\text{O}$, the method developed by Kellogg,⁶⁰ which consists in summing the various contributions from cationic and anionic groups in compounds (i.e., $C_p^0(298.15\text{K}) = \sum[\theta(\text{cations}) + \theta(\text{anions})]$), was utilized and yielded values of 118.0 J.mol⁻¹.K⁻¹ for $\text{UO}_3 \cdot \text{H}_2\text{O}$ and 109.0 J.mol⁻¹.K⁻¹ for $\text{UO}_3 \cdot 0.75\text{H}_2\text{O}$, using a cationic contribution of $\theta(\text{U}) = 26.78$ J.mol⁻¹.K⁻¹ and anionic contributions of $\theta(\text{O}) = 18.41$ J.mol⁻¹.K⁻¹ and $\theta(\text{H}) = 8.79$ J.mol⁻¹.K⁻¹. Kellogg's C_p^0 estimate for $\text{UO}_3 \cdot \text{H}_2\text{O}$ is 3.5% larger than the corresponding calorimetry value reported by Gurevich *et al.*³⁴ and 5.3 % larger than the value calculated with DFPT in this study, while Kellogg's estimate for $\text{UO}_3 \cdot 0.75\text{H}_2\text{O}$ is $C_p^0 = 109.0$ J.mol⁻¹.K⁻¹, i.e., reproducing the value extrapolated by Hemingway for stoichiometric α -type $\text{UO}_3 \cdot \text{H}_2\text{O}$. Therefore, it can be inferred that, near room temperature, the heat capacity estimates of α -type dehydrated schoepite corrected by Hemingway³² to the compositions of $\text{UO}_3 \cdot 0.85\text{H}_2\text{O}$ and $\text{UO}_3 \cdot \text{H}_2\text{O}$ may be underestimated.

C_p computed with DFPT is 115.4 J.mol⁻¹.K⁻¹ at 316 K, the highest temperature probed by Gurevich *et al.*³⁴ with a measured heat capacity of 117.0 J.mol⁻¹.K⁻¹ (-1.3%) for α -type $\text{UO}_3 \cdot \text{H}_2\text{O}$. However, the calculated isobaric molar heat capacity is larger than the corresponding estimates by Hemingway³² for α -type $\text{UO}_3 \cdot \text{H}_2\text{O}$ between 360 K and 507 K, with computed values of 122.8 and 139.4 J.mol⁻¹.K⁻¹, respectively, and DFPT predictions tend to underestimate experimental results by less than 0.8% over the temperature range 507–650 K. Let us note that an upper temperature limit of 650 K was chosen in this study owing to the approximate thermal stability field of ~ 95 – 345°C (~ 368 – 618 K) reported by Finch *et al.* for α - $\text{UO}_2(\text{OH})_2$ in water.¹² Heating dehydrated schoepite beyond its thermal stability limit usually results in the formation of UO_3 and, eventually, of U_3O_8 .²⁵ At 650 K, the calculated C_p value of 150.3 J.mol⁻¹.K⁻¹ remains ca. 14% below the Dulong-Petit asymptotic value of $C_p = nR = 174.6$ J.mol⁻¹.K⁻¹, where n is the number of atoms per f.u. and R is the universal gas constant.

Moreover, as shown in Fig. 4, DFPT predictions of C_p for α - $\text{UO}_2(\text{OH})_2$ in this study are in overall better agreement with the calorimetry data of Gurevich *et al.*³⁴ and estimates provided by Hemingway³² than previous first-principles calculations using dispersion-interaction corrections (DFPT-D2), which systematically underestimate empirical heat capacity.^{35,36} For example, the standard molar heat capacity C_p^0 predicted with DFPT-D2 by Weck and Kim³⁵ and by Colmenero *et al.*³⁶ are 107.21 and 103.85 J.mol⁻¹.K⁻¹, i.e., underestimating the experimental value of Gurevich *et al.*³⁴ by -5.9% and -8.9%, respectively. Near 650 K, differences larger than 10% appear between DFPT-D2 predictions by Colmenero *et al.*³⁶ and the C_p values extrapolated by Hemingway for stoichiometric α - $\text{UO}_2(\text{OH})_2$. Such simple corrections, using semi-empirical pairwise force field potentials to represent dispersion interactions, are typically optimized to improve the description of low-temperature crystalline structures, but may lead to inaccurate prediction of thermal properties at higher temperature, for which force-field parameters are not optimized.

The thermal variation of the isobaric molar heat capacity of the β - and γ - $\text{UO}_2(\text{OH})_2$ polymorphs calculated in this study is also depicted in Fig. 4. The predicted C_p of the β phase is systematically larger than α - $\text{UO}_2(\text{OH})_2$ for temperatures below ~ 320 K, and the heat capacity of the lowest-density γ - $\text{UO}_2(\text{OH})_2$ polymorph is consistently smaller than other polymorphs. The standard molar heat capacity values predicted with DFPT for β - and γ - $\text{UO}_2(\text{OH})_2$ are $C_p^0 = 112.4 \text{ J}\cdot\text{mol}^{-1}\cdot\text{K}^{-1}$ and $104.8 \text{ J}\cdot\text{mol}^{-1}\cdot\text{K}^{-1}$, respectively. These values are 4.7% and 11.2% smaller than Kellogg's C_p^0 estimate for $\text{UO}_2(\text{OH})_2$.

Fig. 5 shows the thermal variation of the molar entropy of α -, β - and γ - $\text{UO}_2(\text{OH})_2$ polymorphs calculated here with DFPT, along with previous DFPT-D2 calculations by Weck and Kim³⁵ and by Colmenero *et al.*³⁶ and calorimetry estimates for $\text{UO}_3\cdot x\text{H}_2\text{O}$ ($x = 0.64, 0.85, 0.90, 1.00$) reported by Hemingway³², O'Hare *et al.*³³ and Gurevich *et al.*³⁴

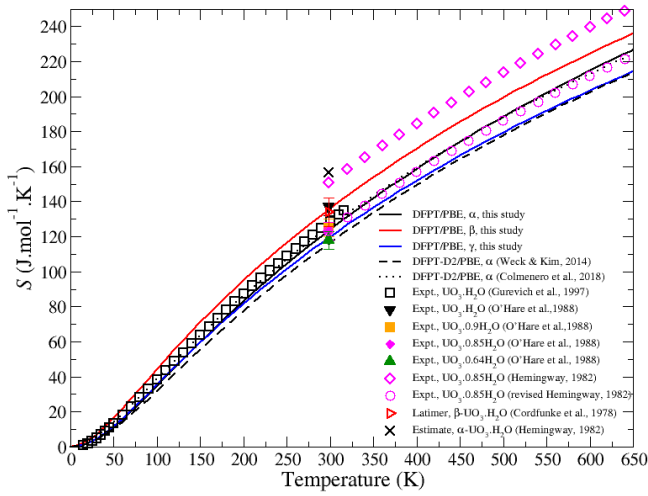


Fig. 5 Thermal variation of the molar entropy of α -, β - and γ - $\text{UO}_2(\text{OH})_2$ polymorphs calculated with DFPT at the GGA/PBE level of theory. DFPT-D2/GGA/PBE calculations for α - $\text{UO}_2(\text{OH})_2$ (Weck and Kim, 2014) and calorimetry estimates for $\text{UO}_3\cdot x\text{H}_2\text{O}$ ($x = 0.64, 0.85, 0.90, 1.00$) are also shown for comparison purpose (Hemingway, 1982; O'Hare *et al.*, 1988; Gurevich *et al.*, 1997).

The standard molar entropy values of α -, β - and γ - $\text{UO}_2(\text{OH})_2$ obtained here using DFPT are $S^0 = 123.1, 135.3$ and $119.0 \text{ J}\cdot\text{mol}^{-1}\cdot\text{K}^{-1}$, respectively. These predictions are close to the experimental estimate of $S^0 = 128.10 \pm 0.20 \text{ J}\cdot\text{mol}^{-1}\cdot\text{K}^{-1}$ reported by Gurevich *et al.*³⁴ for α - $\text{UO}_2(\text{OH})_2$, as well as the calorimetry data by O'Hare *et al.*³³ ranging from $S^0 = 137 \pm 5 \text{ J}\cdot\text{mol}^{-1}\cdot\text{K}^{-1}$ for stoichiometric $\text{UO}_3\cdot\text{H}_2\text{O}$ to $118 \pm 5 \text{ J}\cdot\text{mol}^{-1}\cdot\text{K}^{-1}$ for $\text{UO}_3\cdot 0.64\text{H}_2\text{O}$ and Latimer's estimate of $S^0 = 134 \pm 8 \text{ J}\cdot\text{mol}^{-1}\cdot\text{K}^{-1}$ for β - $\text{UO}_2(\text{OH})_2$ provided by Cordfunke and O'Hare.³¹ Here, the standard entropy of $\text{UO}_2(\text{OH})_2$ was estimated using Latimer's rule^{61,62} according to:

$$S^0 = S(298.15 \text{ K}) = \left(\frac{3R}{2}\right) (\ln M_U + 4 \ln M_O + 2 \ln M_H) + 7 R s', \quad (5)$$

where $R = 8.3145 \text{ J}\cdot\text{mol}^{-1}\cdot\text{K}^{-1}$ is the universal gas constant, the constant $s' = -0.94$ was determined empirically by Latimer from the standard entropy of KCl, and M_U, M_O and M_H are the atomic masses of U, O and H, respectively. For stoichiometric

$\text{UO}_3\cdot\text{H}_2\text{O}$ (i.e., $\text{UO}_2(\text{OH})_2$), Latimer's estimate is predicted to be $S^0 = 152.05 \text{ J}\cdot\text{mol}^{-1}\cdot\text{K}^{-1}$, while for $\text{UO}_3\cdot 0.75\text{H}_2\text{O}$ Latimer's rule yields $S^0 = 149.22 \text{ J}\cdot\text{mol}^{-1}\cdot\text{K}^{-1}$. This Latimer's estimate for $\text{UO}_2(\text{OH})_2$ is in line with the value of $156.6 \text{ J}\cdot\text{mol}^{-1}\cdot\text{K}^{-1}$ derived by Hemingway³² based on a combination of reaction data by Sergeyeva *et al.*⁶³ and other thermodynamic data from Robie *et al.*⁶⁴ and adjusted compositionally through addition of appropriate amount of H_2O as steam at the temperature of the experimental data point. Such compositional adjustment was made because H_2O in this material was shown in previous studies to behave approximatively like zeolitic water,⁶⁵ and this approximation was believed to be valid within the experimental error of the DSC values. Similarly, Hemingway estimated $S^0 = 150.7 \text{ J}\cdot\text{mol}^{-1}\cdot\text{K}^{-1}$ for α -type $\text{UO}_3\cdot 0.85\text{H}_2\text{O}$ and provided extrapolated molar entropy values to 700 K.³² However, as shown in Fig. 5, the standard molar entropy provided by Hemingway³² for $\text{UO}_3\cdot 0.85\text{H}_2\text{O}$ is $\sim 22.5\%$ larger than the corresponding value of O'Hare *et al.*³³ However, applying a $-27.7 \text{ J}\cdot\text{mol}^{-1}\cdot\text{K}^{-1}$ shift ($\Delta S^0 = 123 - 150.7 \text{ J}\cdot\text{mol}^{-1}\cdot\text{K}^{-1}$) to entropy results given by Hemingway to close the gap between S^0 values of O'Hare *et al.* and Hemingway results in better revised molar entropy estimates (see magenta open circles in Fig. 5).

The thermal variations of the isobaric molar heat capacity C_p calculated with DFPT for α -, β - and γ - $\text{UO}_2(\text{OH})_2$ polymorphs were fitted in the temperature range 100–650 K using nonlinear least-squares regression to a Haas-Fisher-type polynomial,

$$C_p(T) = a + bT + cT^{-2} + dT^{-0.5} + eT^2, \quad (6)$$

with the resulting optimized coefficients summarized in Table 2. The sum of squared differences (SSD) between DFPT-calculated and fitted data remained below 0.35 over the temperature range considered for all polymorphs.

Table 2. Coefficients of the Haas-Fisher isobaric molar heat capacity polynomial $C_p(T)$ for α -, β - and γ - $\text{UO}_2(\text{OH})_2$ polymorphs calculated with DFPT at the GGA/PBE level of theory. The range of validity of the fit is 100–650 K.

	$a \times 10^2$ (T^0)	$b \times 10^{-1}$ (T)	$c \times 10^4$ (T^{-2})	$d \times 10^2$ ($T^{-0.5}$)	$e \times 10^{-4}$ (T^2)	SSD ^a
α	1.0971	2.0777	1.024871	-7.9375	-1.545	0.25
β	1.3031	1.6305	7.235009	-9.6752	-1.273	0.34
γ	1.1127	1.7974	5.242618	-8.3219	-1.411	0.33

^a Sum of squared differences between calculated and fitted data.

Using the coefficients of the Haas-Fisher polynomials in Table 2, the enthalpy function, $(H_T - H_{298.15})\cdot T^{-1}$, was obtained for α -, β - and γ - $\text{UO}_2(\text{OH})_2$ polymorphs by analytical integration of the fit to the isobaric heat capacity according to the formula:

$$(H_T - H_{298.15})\cdot T^{-1} = \int_{298.15}^T (a + bT + cT^{-2} + dT^{-0.5} + eT^2) dT. \quad (7)$$

Fig. 6 displays the calculated molar enthalpy function of stoichiometric α -, β - and γ - $\text{UO}_2(\text{OH})_2$, along with experimental estimates for α -type $\text{UO}_3\cdot 0.85\text{H}_2\text{O}$ derived from calorimetric data by Hemingway³² and the DFPT-D2 results for α - $\text{UO}_2(\text{OH})_2$ by Weck and Kim³⁵ and by Colmenero *et al.*³⁶ Similar to previous

findings for C_p , the calculated molar enthalpy functions of α - and β - $\text{UO}_2(\text{OH})_2$ are very close, while values for the lowest-density phase γ - $\text{UO}_2(\text{OH})_2$ appear significantly smaller (-6.4% and -7.1% smaller than the corresponding values for the β and α polymorphs at 500 K). The α - $\text{UO}_2(\text{OH})_2$ molar enthalpy function values calculated with DFPT in this study are systematically larger by several percents than previous DFPT-D2 results accounting for dispersion correction interactions. At 500 K, for example, the molar enthalpy function value predicted in this study is 3.9% and 4.8% larger than values obtained by Colmenero *et al.*³⁶ and Weck and Kim,³⁵ respectively. As expected, the present DFPT predictions for α - $\text{UO}_2(\text{OH})_2$ slightly overestimate the experimental values for α -type $\text{UO}_3 \cdot 0.85\text{H}_2\text{O}$ derived from calorimetric data by Hemingway,³² with differences of up to 2.4% near 640 K.

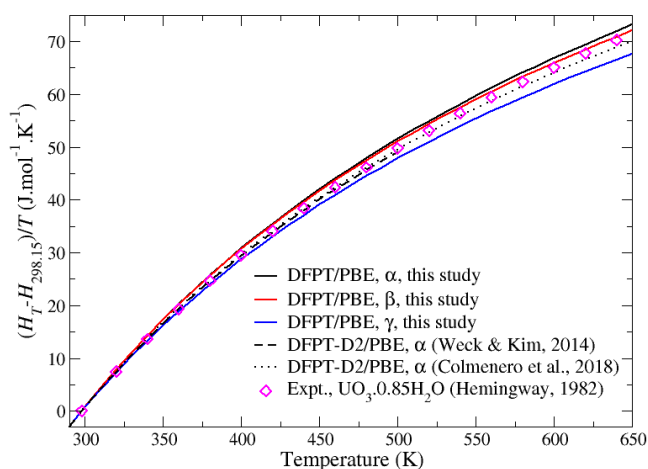


Fig. 6 Thermal variation of the molar enthalpy function of α -, β - and γ - $\text{UO}_2(\text{OH})_2$ polymorphs calculated with DFPT at the GGA/PBE level of theory. DFPT-D2/GGA/PBE calculations for α - $\text{UO}_2(\text{OH})_2$ (Weck and Kim, 2014; Colmenero *et al.*, 2018) and calorimetry estimates for α -type $\text{UO}_3 \cdot 0.85\text{H}_2\text{O}$ are also shown for comparison (Hemingway, 1982).

Finally, the Gibbs energy function, $-(G_T - H_{298.15}) \cdot T^{-1}$, was obtained using the expression:

$$-(G_T - H_{298.15}) \cdot T^{-1} = S_T - (H_T - H_{298.15}) \cdot T^{-1}, \quad (8)$$

where S_T is the molar entropy obtained by integration of the isobaric molar heat capacity according to Eq. (4). Fig. 7 shows the DFPT-computed molar enthalpy functions of stoichiometric α -, β - and γ - $\text{UO}_2(\text{OH})_2$, with original and revised experimental estimates for α -type $\text{UO}_3 \cdot 0.85\text{H}_2\text{O}$ provided by Hemingway,³² as well as the DFPT-D2 results for α - $\text{UO}_2(\text{OH})_2$ by Weck and Kim³⁵ and by Colmenero *et al.*³⁶ The standard molar Gibbs energy function values predicted with DFPT are 123.1, 135.2 and 119.0 $\text{J} \cdot \text{mol}^{-1} \cdot \text{K}^{-1}$ for α -, β - and γ - $\text{UO}_2(\text{OH})_2$ polymorphs, respectively. The standard value calculated here for α - $\text{UO}_2(\text{OH})_2$ is 6.0% larger than the corresponding DFPT-D2 prediction of Weck and Kim³⁵, although it is smaller by -1.6% than the DFPT-D2 estimate by Colmenero *et al.*³⁶ Those differences between the present DFPT result and the previous

DFPT-D2 calculations of Weck and Kim and Colmenero *et al.* are consistent with the corresponding standard entropy differences of +6.0% and -1.7% shown in Fig. 5 for α - $\text{UO}_2(\text{OH})_2$. As depicted in Fig. 6, differences in enthalpy functions between the present calculations and previous DFPT-D2 results for α - $\text{UO}_2(\text{OH})_2$ are relatively small, and the entropy term in Eq. (8) is responsible for the largest differences between the Gibbs energy functions.

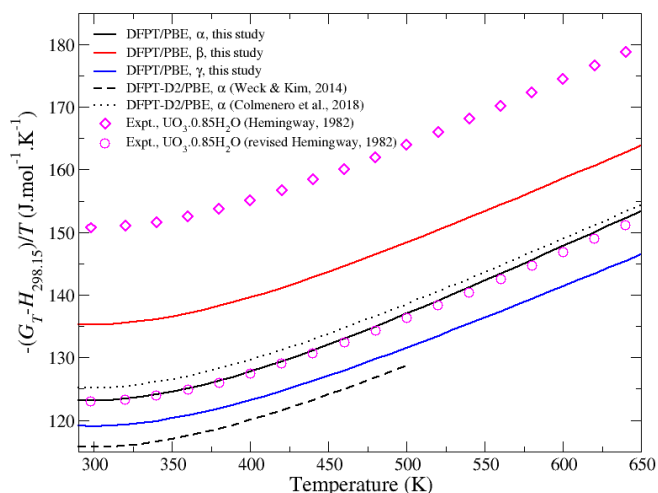


Fig. 7 Thermal variation of the molar Gibbs energy function of α -, β - and γ - $\text{UO}_2(\text{OH})_2$ polymorphs calculated with DFPT at the GGA/PBE level of theory. DFPT-D/GGA/PBE calculations for α - $\text{UO}_2(\text{OH})_2$ (Weck and Kim, 2014) and calorimetry estimates for $\text{UO}_3 \cdot 0.85\text{H}_2\text{O}$ are also shown for comparison (Hemingway, 1982).

In addition, as discussed above, applying a $\Delta S^0 = -27.7 \text{ J} \cdot \text{mol}^{-1} \cdot \text{K}^{-1}$ shift to the original entropy estimates by Hemingway leads to a standard molar Gibbs energy function value of 123.0 $\text{J} \cdot \text{mol}^{-1} \cdot \text{K}^{-1}$ for $\text{UO}_3 \cdot 0.85\text{H}_2\text{O}$, significantly improving the agreement with the DFPT value predicted in this study for α - $\text{UO}_2(\text{OH})_2$.

Conclusions

In summary, the phase transitions and thermodynamics of stoichiometric dehydrated schoepite α -, β -, and γ - $\text{UO}_2(\text{OH})_2$ polymorphs were investigated within the framework of density functional perturbation theory. The lowest-density monoclinic γ polymorph is the most energetically favorable phase, followed by the orthorhombic β phase, and the orthorhombic α phase. The pressure-induced $\beta(Pbca) \rightarrow \alpha(Cmca)$ and $\gamma(P2_1/c) \rightarrow \alpha(Cmca)$ phase transitions from open octahedral structures with six O atoms coordinated to U metal centers to puckered hexagonal sheets with 8-coordinated U atoms, lead to theoretical volume reductions of $\Delta V/V = -14.7\%$ and -16.4% , respectively. This computational result for the $\beta \rightarrow \alpha$ martensitic-like phase transformation exactly matches the volume contraction value measured by dilatometry and XRD techniques. Calculations show that γ and β polymorphs become energetically degenerate upon compression as they convert to the α polymorph, explaining the presence of β - and γ - $\text{UO}_2(\text{OH})_2$ mixtures in grinding experiments. In addition, Gibbs free energy calculations predict the temperature-driven $\gamma \rightarrow \beta$ phase transition to occur in the vicinity of 533 K, consistent with the

experimental observation of a major change of the crystal unit-cell angle near 553 K.

The thermodynamic properties of α -, β -, and γ - $\text{UO}_2(\text{OH})_2$, such as the molar isobaric heat capacity, entropy, enthalpy and Gibbs energy functions, were computed using phonon frequencies calculated with DFPT. At 298.15 K, the predicted standard molar heat capacity for α - $\text{UO}_2(\text{OH})_2$ is $C_p^0 = 112.1 \text{ J}\cdot\text{mol}^{-1}\cdot\text{K}^{-1}$, i.e., only 1.6% smaller than the calorimetry value of $C_p^0 = 113.96 \pm 0.12 \text{ J}\cdot\text{mol}^{-1}\cdot\text{K}^{-1}$, and $C_p^0 = 112.4$ and $104.8 \text{ J}\cdot\text{mol}^{-1}\cdot\text{K}^{-1}$ for β - and γ - $\text{UO}_2(\text{OH})_2$, respectively. The standard molar entropy values of α -, β - and γ - $\text{UO}_2(\text{OH})_2$ obtained in this study are $S^0 = 123.1$, 135.3 and $119.0 \text{ J}\cdot\text{mol}^{-1}\cdot\text{K}^{-1}$, respectively. These predictions are in close agreement with the experimental estimate of $S^0 = 128.10 \pm 0.20 \text{ J}\cdot\text{mol}^{-1}\cdot\text{K}^{-1}$ reported by Gurevich *et al.* for α - $\text{UO}_2(\text{OH})_2$, as well as the calorimetry data by O'Hare *et al.* ranging from $S^0 = 137 \pm 5 \text{ J}\cdot\text{mol}^{-1}\cdot\text{K}^{-1}$ for $\text{UO}_3\cdot\text{H}_2\text{O}$ to $118 \pm 5 \text{ J}\cdot\text{mol}^{-1}\cdot\text{K}^{-1}$ for $\text{UO}_3\cdot 0.64\text{H}_2\text{O}$ and Latimer's estimate of $S^0 = 134 \pm 8 \text{ J}\cdot\text{mol}^{-1}\cdot\text{K}^{-1}$ for β - $\text{UO}_2(\text{OH})_2$ provided by Cordfunke and O'Hare.

Finally, based on the present DFPT calculations and existing calorimetry data, applying a $\Delta S^0 = -27.7 \text{ J}\cdot\text{mol}^{-1}\cdot\text{K}^{-1}$ shift to entropy results given by Hemingway is proposed here to close the gap between S^0 values of O'Hare *et al.* and Hemingway and to provide better molar entropy estimates at high temperature. DFPT calculations suggest that a reexamination of the high-temperature calorimetric data of dehydrated schoepite polymorphs might be necessary.

Conflicts of interest

There are no conflicts to declare.

Data availability

Data for this article are available in accordance with DOE Policy for Digital Research Data Management. The DOE will provide public access to results of federally sponsored research in accordance with the DOE Public Access Plan.

<https://www.energy.gov/datamanagement/doe-policy-digital-research-data-management>

Acknowledgements

Sandia National Laboratories is a multi-mission laboratory managed and operated by National Technology & Engineering Solutions of Sandia, LLC (NTESS), a wholly owned subsidiary of Honeywell International Inc., for the U.S. Department of Energy's National Nuclear Security Administration (DOE/NNSA) under contract DE-NA0003525. This written work is authored by an employee of NTESS. The employee, not NTESS, owns the right, title and interest in and to the written work and is responsible for its contents. Any subjective views or opinions that might be expressed in the written work do not necessarily represent the views of the U.S. Government. The publisher acknowledges that the U.S. Government retains a non-exclusive, paid-up, irrevocable, world-wide license to publish or reproduce the published form of this written work or allow others to do so, for U.S. Government purposes. The DOE will provide public access to results of federally sponsored research in accordance with the DOE Public Access Plan. This work was supported by the Spent Fuel and Waste Science and Technology (SFWST) Campaign and the Nuclear Energy University Program (NEUP) of the U.S. DOE Office of Nuclear Energy (NE).

References

- ¹ R. J. Baker, *Coord. Chem. Rev.*, 2014, 266-267, 123.
- ² R. J. Finch, E. C. Buck, P. A. Finn, J. K. Bates, *Mat. Res. Soc. Symp. Proc.*, 1999, **556**, 431.
- ³ T. Wadsen, *J. Nucl. Mater.*, 1977, **64**, 315.
- ⁴ E. C. Buck, D. J. Wronkiewicz, P. A. Finn, J. K. Bates, *J. Nucl. Mater.*, 1997, **249**, 70.
- ⁵ C. L. Christ, J. R. Clark, *Am. Mineral.*, 1960, **45**, 1026.
- ⁶ H. T. Evans, *Science*, 1963, **141**, 154.
- ⁷ M. L. Miller, R. J. Finch, P. C. Burns, R. C. Ewing, *J. Mater. Res.*, 1996, **11**, 3048.
- ⁸ P. C. Burns, M. L. Miller, R. C. Ewing, *Can. Mineral.*, 1996, **34**, 845.
- ⁹ R. J. Finch, M. A. Cooper, F. C. Hawthorne, *Can. Mineral.*, 1996, **34**, 1071.
- ¹⁰ M. T. Weller, M. E. Light, T. Gelbrich, *Acta Crystallogr.*, 2000, **B56**, 577.
- ¹¹ J. C. Taylor, H. J. Hurst, *Acta Crystallogr.*, 1971, **B27**, 2018.
- ¹² R. J. Finch, F. C. Hawthorne, R. C. Ewing, *Can. Mineral.*, 1998, **36**, 831.
- ¹³ I. G. Draganic, Z. D. Draganic, *The Radiation Chemistry of Water*, Academic Press, New York, 1971.
- ¹⁴ G. Sattonnay, C. Ardois, C. Corbel, J.-F. Lucchini, M.-F. Barthe, F. Garrido, D. Gosset, *J. Nucl. Mater.*, 2001, **288**, 11.
- ¹⁵ M. Amme, *Radiochim. Acta*, 2002, **90**, 399.

-
- ¹⁶ B. McNamara, B. Hanson, B. E. Buck, *Mater. Res. Soc. Symp. Proc.*, 2003, **757**, 401.
- ¹⁷ B. Hanson, B. McNamara, B. E. Buck, J. Friese, E. Jenson, K. Krupka, B. Arey, *Radiochim. Acta*, 2005, **93**, 159.
- ¹⁸ B. McNamara, B. Hanson, E. Buck, C. Soderquist, *Radiochim. Acta*, 2005, **93**, 169.
- ¹⁹ T. Z. Forbes, P. Horan, T. Devine, D. McInnis, P. C. Burns, *Am. Mineral.*, 2011, **96**, 202.
- ²⁰ J. K. Dawson, E. Wait, K. Alcock, D. R. Chilton, *J. Chem. Soc.*, 1956, 3531.
- ²¹ E. H. P. Cordfunke, P. C. Debets, *J. Inorg. Nucl. Chem.*, 1964, **26**, 1671.
- ²² M. J. Bannister, J. C. Taylor, *Acta Crystallogr.*, 1970, **B26**, 1775.
- ²³ J. C. Taylor, *Acta Crystallogr.*, 1971, **B27**, 1088.
- ²⁴ J. C. Taylor, J. W. Kelly, B. Downer, *J. Solid State Chem.*, 1972, **5**, 291.
- ²⁵ R. B. Roof, D. T. Cromer, A. C. Larson, *Acta Crystallogr.*, 1964, **17**, 710.
- ²⁶ S. Siegel, H. R. Hoekstra, E. Gebert, *Acta Crystallogr.*, 1972, **B28**, 3469.
- ²⁷ D. K. Smith, B. E. Scheetz, C. A. F. Anderson, K. L. Smith, *Uranium*, 1982, **1**, 79.
- ²⁸ J. Brugger, N. Meisser, B. Etschmann, S. Ansermet, A. Pring, *Am. Mineral.*, 2011, **96**, 229.
- ²⁹ L. A. Harris, A. J. Taylor, *J. Am. Ceram. Soc.*, 1962, **45**, 25.
- ³⁰ H. R. Hoekstra, S. Siegel, *J. Inorg. Nucl. Chem.*, 1973, **35**, 761.
- ³¹ E. H. P. Cordfunke, P. A. G. O'Hare, *The chemical thermodynamics of actinide elements and compounds. Part 3. Miscellaneous actinide compounds*: International Atomic Energy Agency, Vienna, Austria, 1978, p. 83.
- ³² B. S. Hemingway, *Thermodynamic properties of selected uranium compounds and aqueous species at 298.15 K and 1 bar and at higher temperatures; preliminary models for the origin of coffinite deposits*, USGS Open-File Report 82-619, 1982.
- ³³ P. A. G. O'Hare, B. M. Lewis, S. N. Nguyen, *J. Chem. Thermodynamics*, 1988, **20**, 1287.
- ³⁴ V. M. Gurevich, E. I. Sergeeva, K. S. Gavrichev, V. E. Gorbunov, T. P. Kuznetsova, I. L. Khodakovskii, *Geokhimiya*, 1997, **1**, 82.
- ³⁵ P. F. Weck, E. Kim, *Dalton Trans.*, 2014, **43**, 17191.
- ³⁶ F. Colmenero, A. M. Fernandez, J. Cobos, V. Timon, *J. Phys. Chem. C*, 2018, **122**, 5254.
- ³⁷ G. Kresse, J. Furthmüller, *Phys. Rev. B*, 1996, **54**, 11169.
- ³⁸ J. P. Perdew, J. A. Chevary, S. H. Vosko, K. A. Jackson, M. R. Pederson, D. J. Singh, C. Fiolhais, *Phys. Rev. B*, 1992, **46**, 6671.
- ³⁹ J. P. Perdew, K. Burke, M. Ernzerhof, *Phys. Rev. Lett.*, 1996, **77**, 3865.
- ⁴⁰ P. F. Weck, E. Kim, N. Balakrishnan, F. Poineau, C. B. Yeaman, K. R. Czerwinski, *Chem. Phys. Lett.*, 2007, **443**, 82.
- ⁴¹ P. F. Weck, E. Kim, B. Masci, P. Thuery, K. R. Czerwinski, *Inorg. Chem.*, 2010, **49**, 1465.
- ⁴² P. F. Weck, C.-M. S. Gong, E. Kim, P. Thuery, K. R. Czerwinski, *Dalton Trans.*, 2011, **40**, 6007.
- ⁴³ P. F. Weck, E. Kim, C. F. Jové-Colón, D. C. Sassani, *Dalton Trans.*, 2012, **41**, 9748.
- ⁴⁴ P. F. Weck, E. Kim, C. F. Jové-Colón, D. C. Sassani, *Dalton Trans.*, 2013, **41**, 4570.
- ⁴⁵ S. Ostanin, P. Zeller, *J. Phys.: Condens. Matter*, 2007, **19**, 246108.
- ⁴⁶ S. Ostanin, P. Zeller, *Phys. Rev. B*, 2007, **75**, 073101.
- ⁴⁷ P. F. Weck, C. F. Jové-Colón, Kim E., *Phys. Chem. Chem. Phys.*, 2023, **25**, 16727.
- ⁴⁸ P. F. Weck, C. F. Jové-Colón, E. Kim, *Phys. Chem. Chem. Phys.*, 2019, **21**, 25569.
- ⁴⁹ P. F. Weck, C. F. Jové-Colón, E. Kim, *Chem. Phys. Lett.*, 2020, **757**, 137878.
- ⁵⁰ P. E. Blöchl, *Phys. Rev. B*, 1994, **50**, 17953.
- ⁵¹ G. Kresse, D. Joubert, *Phys. Rev. B*, 1999, **59**, 1758.
- ⁵² E. R. Davidson, *Methods in Computational Molecular Physics*, G. H. F. Diercksen and S. Wilson, Eds., Vol. 113, NATO Advanced Study Institute, Series C, Plenum, New York, 1983, p. 95.
- ⁵³ H. J. Monkhorst, J. D. Pack, *Phys. Rev. B*, 1976, **13**, 5188.
- ⁵⁴ P. Blöchl, O. Jepsen, O. Andersen, *Phys. Rev. B*, 1994, **49**, 16223.
- ⁵⁵ A. Togo, F. Oba, I. Tanaka, *Phys. Rev. B*, 2008, **78**, 134106.
- ⁵⁶ X. Wu, M. C. Vargas, S. Nayak, V. Lotrich, G. Scoles, *J. Chem. Phys.*, 2001, **115**, 8748.
- ⁵⁷ S. Grimme, *J. Comp. Chem.*, 2006, **27**, 1787.
- ⁵⁸ R. V. Lindval', V. V. Kuznetsova, *Tr. Kazan. Khim. Tekhnol. Inst.*, 1974, **54**, 145.
- ⁵⁹ J. A. Perez-Bustamante, J. B. Polonio, R. F. Cellini, *Anal. Real. Soc. Espan. Fis. Quim.*, 1962, **B58**, 677.
- ⁶⁰ H. H. Kellogg, in *Applications of Fundamental Thermodynamics to Metallurgical Processes*, Gordon and Breach, 1967, 357.
- ⁶¹ W. M. Latimer, *J. Am. Chem. Soc.*, 1921, **43**, 818.
- ⁶² G. Grimvall, *Int. J. Thermophysics*, 1983, **4**, 363.
- ⁶³ E. I. Sergeeva, A. A. Nikitin, I. L. Khodakovskiy, G. B. Naumov, *Geochemistry International*, 1972, **9**, 900.
- ⁶⁴ R. A. Robie, B. S. Hemingway, J. R. Fisher, *Thermodynamic properties of minerals and related substances at 298.15 K and 1 bar (10⁵ pascals) pressure and at higher temperatures (revised edition)*, U.S. Geol. Survey Bull. 1452, 1979, p. 456.
- ⁶⁵ A. L. Porte, H. S. Gutowsky, J. E. Boggs, *J. Chem. Phys.*, 1962, **36**, 1695; **36**, 1700.